at 100 K. The largest modulation amplitudes ($\simeq$0.04 Å) are on Mo(2) and Mo(3) atoms forming the infinite chain along **b**. Their displacements are in the slabs and perpendicular to **b**. Within one slab, all Mo atoms, which are on the same height in the chain, displace in phase. With a phase shift of 90°, the alkali atoms together with their surrounding oxygens displace ($\sim$0.02 Å) in the chain direction. Displacements in neighbouring layers are in antiphase. The same structural features are observed for both the K and and the Rb bronzes.

Charge-distribution calculations in the modulated structure reveal valence fluctuations on the Mo atoms along the chain direction by varying Mo–O bonding. The Mo^{5+} ordering below T_c on the Mo(2), Mo(3) atoms and the charge transfer within the $Mo_{10}O_{30}$ cluster, together with a varying orbital overlap along the chain direction, point to localization of conduction electrons and are probably the origin of the nonlinear transport properties.

This work is part of the research program of the Netherlands Foundation for Chemical Research (SON) and was made possible by financial support from the Netherlands Organisation for the Advancement of Pure Research (ZWO). This work was supported in part by the EC contract No. SC1-0032-C(CD).

References

BOER, J. L. DE & DUISENBERG, A. J. M. (1984). *Enraf–Nonius CAD-4F Diffractometer Software Update*, February 1984. Enraf–Nonius, Groningen and Utrecht, The Netherlands.

BROWN, D. (1981). *Structure and Bonding in Crystals*, Vol. II, edited by M. O'KEEFFE & A. NAVROTSKY, pp. 1–30. New York: Academic Press.

COLAITIS, D. (1989). *J. Solid State Chem.* **83**, 158–169.

DUMAS, J., SCHLENKER, C., MARCUS, J. & BUDER, R. (1983). *Phys. Rev. Lett.* **50**, 757–760.

GANNE, M., BOUMAZA, A., DION, M. & DUMAS, J. (1985). *Mater. Res. Bull.* **20**, 1297–1308.

GHEDIRA, M., CHENAVAS, J., MAREZIO, M. & MARCUS, J. (1985). *J. Solid State Chem.* **57**, 300–313.

GOODENOUGH, J. B. (1965). *Bull. Soc. Chim. Fr.* **4**, 1200–1207.

GOODENOUGH, J. B. (1970). *J. Solid State Chem.* **1**, 349–358.

GRAHAM, J. & WADSLEY, A. D. (1966). *Acta Cryst.* B**20**, 93–100.

GRÜNER, G. (1988). *Rev. Mod. Phys.* **60**, 1129–1181.

HALL, S. R. & STEWART, J. M. (1987). Editors. *XTAL2.2 Users Manual*. Univs. of Western Australia, Australia, and Maryland, USA.

HUTIRAY, G. & SOLYOM, J. (1985). *Charge Density Waves in Solids*, Springer Lecture Notes in Physics Vol. 217, pp. 17–22, 439–448. Berlin: Springer Verlag.

JANNER, A., JANSSEN, T. & DE WOLFF, P. M. (1983). *Acta Cryst.* A**39**, 671–678.

MUMME, W. G. & WATTS, J. A. (1970). *J. Solid State Chem.* **2**, 16–23.

POUGET, J. P., NOGUERA, C., MOUDDEN, A. H. & MORET, R. (1985). *J. Phys. (Paris)*, **46**, 1731–1742.

SATO, M., FUJISHITA, H., SATO, S. & HOSHINO, S. (1985). *J. Phys. C*, **18**, 2603–2614.

SCHLENKER, C. (1989). *Low-Dimensional Electronic Properties of Molybdenum Bronzes and Oxides*, edited by C. SCHLENKER, pp. 159–252. Dordrecht: Kluwer Academic Publishers.

SCHLENKER, C. & DUMAS, J. (1986). *Crystal Chemistry and Properties of Materials with Quasi-One-Dimensional Structures*, edited by J. ROUXEL, pp. 135–177. Dordrecht: Reidel.

SCHUTTE, W. J. & DE BOER, J. L. (1988). *Acta Cryst.* B**44**, 486–494.

SCHUTTE, W. J. & DE BOER, J. L. (1993). *Acta Cryst.* B**49**. In the press.

SEGRANSAN, P., JANOSSY, A., BERTHIER, C., MARCUS, J. & BUTAUD, P. (1986). *Phys. Rev. Lett.* **56**, 1854–1857.

SMAALEN, S. VAN, BRONSEMA, K. D. & MAHY, J. (1986). *Acta Cryst.* B**42**, 43–50.

STEPHENSON, N. C. & WADSLEY, A. D. (1965). *Acta Cryst.* **19**, 241–247.

TRAVAGLINI, G. & WACHTER, P. (1983). *Solid State Commun.* **47**, 217–221.

TSAI, P. P., POTENZA, J. A. & GREENBLATT, M. (1987). *J. Solid State Chem.* **69**, 329–335.

WOLFF, P. M. DE, JANSSEN, T. & JANNER, A. (1981). *Acta Cryst.* A**37**, 625–636.

YAMAMOTO, A. (1985). *REMOS85.0. Computer Program for the Refinement of Modulated Structures*. National Institute for Research in Inorganic Materials, Sakura-Mura, Niihari-Gun, Ibaraki 305, Japan.

ZACHARIASEN, W. H. (1978). *J. Less Common Met.* **62**, 1–7.

Acta Cryst. (1993). B**49**, 591–599

Charge Densities of Two Rutile Structures: NiF_2 and CoF_2

BY M. M. R. COSTA, J. A. PAIXÃO, M. J. M. DE ALMEIDA AND L. C. R. ANDRADE

Centro FC1, INIC, Department of Physics, University of Coimbra, 3000 *Coimbra, Portugal*

(*Received* 29 *July* 1992; *accepted* 12 *February* 1993)

Abstract

X-ray diffraction data were collected at room temperature for two rutile structures, NiF_2 and CoF_2. Two different crystals of each compound have been used in the experiments. Atomic and thermal parameters were derived from least-squares refinements of high-angle data [$(\sin\theta)/\lambda \geq 0.6$ Å^{-1}]. The results of

Fourier inversion of the differences between observed and model structure factors are presented and discussed in terms of difference density maps. The observed charge densities are quantitatively interpreted in terms of: (i) occupation of 3*d* orbitals; (ii) multipole analysis. A comparison is made between the results obtained from both models. Finally, the charge density features of a series of rutile structures already investigated are compared and discussed. Crystal data: (*a*) NiF_2, $M_r = 96.71$, tetragonal, $P4_2/mnm$, $a = 4.6497$ (6), $c = 3.0836$ (6) Å, $V = 66.67$ Å^3, $Z = 2$, $D_x = 4.818$ Mg m^{-3}, λ(Mo $K\alpha$) = 0.7017 Å, μ(Mo $K\alpha$) = 705.6 mm^{-1}, $F(000) = 92$, room temperature. Final R values (spherical refinement): 0.013 for 137 independent reflections from crystal *A*; 0.020 for 154 independent reflections from crystal *B*. (*b*) CoF_2, $M_r = 96.93$, tetragonal, $P4_2/mnm$, $a = 4.6950$ (7), $c = 3.1817$ (5) Å, $V = 70.10$ Å^3, $Z = 2$, $D_x = 4.590$ Mg m^{-3}, λ(Mo $K\alpha$) = 0.7017 Å, μ(Mo $K\alpha$) = 586.5 mm^{-1}, $F(000) = 90$, room temperature. Final R values (spherical refinement): 0.019 for 140 independent reflections from crystal *C*; 0.016 for 137 independent reflections from crystal *D*.

Introduction

Both NiF_2 and CoF_2 are rutile structures with transition-metal atoms occupying the corners and the center of a tetragonal unit cell, and the fluorine atoms located at sites $(x, x, 0)$; $(\bar{x}, \bar{x}, 0)$; $(x + \frac{1}{2}, \bar{x} + \frac{1}{2}, \frac{1}{2})$; $(\bar{x} + \frac{1}{2}, x + \frac{1}{2}, \frac{1}{2})$ (Fig. 1). Six of these atoms form the quasi-octahedral environment of the transition-metal atom.

A crystal field with this particular symmetry may disturb the sphericity of the electron distribution around the transition element; if this is the case, a preferential occupation of 3*d* orbitals with particular symmetries should be observed; moreover, any degree of covalency in these ionic structures can be evidenced in a multipole refinement of charge density in the unit cell.

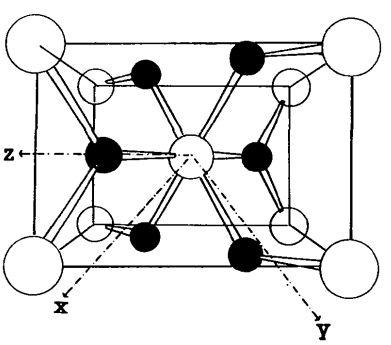

Fig. 1. Unit cell of the rutile structure showing the set of axes for the analysis of 3*d* orbital population. ○ = transition-metal atoms, ● = F atoms.

In order to compare these effects in similar structures as the transition elements vary along the first series, we have now investigated NiF_2 and CoF_2. This complements previous work on rutile structures carried out in our laboratory (Andrade, 1986; Costa & Almeida, 1987; Almeida, Costa & Paixão, 1989).

The conclusions of this study are presented and discussed in the present paper.

Experimental

All X-ray diffraction measurements were carried out on a CAD-4 four-circle automatic diffractometer, at room temperature stabilized within ±2 K.

(*a*) NiF_2

Two sets of X-ray diffraction data were collected from single crystals *A* and *B* (data sets *A* and *B*, respectively). Both crystals were selected from the same bulk material kindly supplied by Dr J. B. Forsyth (Rutherford Appleton Laboratory, Oxford, England), their approximate dimensions being 0.05 × 0.03 × 0.08 mm^3 (crystal *A*) and 0.10 × 0.10 × 0.20 mm^3 (crystal *B*). Lattice parameters were derived from the angular positions of 25 reflections within 2θ ranges of 18–67° for crystal *A* and 24–67° for crystal *B*: $a = b = 4.6497$ (6), $c = 3.0836$ (6) Å.

(*b*) CoF_2

Two single crystals *C* and *D* with polyhedral shapes and approximate dimensions 0.14 × 0.14 × 0.12 mm^3 and 0.12 × 0.12 × 0.10 mm^3, respectively, were selected from a sample kindly supplied by Dr P. J. Brown (Institut Laue–Langevin, Grenoble, France). Lattice parameters were derived from the angular positions of 25 reflections with $30 < 2\theta < 60°$ (crystal *C*) and $19 < 2\theta < 43°$ (crystal *D*): $a = b = 4.6950$ (7), $c = 3.1817$ (5) Å.

Both sets of lattice parameters are in good agreement with those quoted in previous work (Stout & Reed, 1954; Haendler, Patterson & Bernard, 1952).

Relevant information concerning the experimental set-up and measurements is given in Table 1.

All data sets (*A*, *B*, *C* and *D*) include sub-sets of those symmetry-equivalent reflections geometrically accessible, each sub-set containing up to 16 reflections. This enables an absorption correction to be applied and its 'efficiency' to be checked. Five standard reflections were measured every 3 h to check the stability of the main beam; maximum fluctuations of their intensities did not exceed 3% in any experiment (running times varying from 190 to 262 h). In order to correct the integrated intensities for such fluc-

Table 1. *Experimental conditions used in data collections A, B, C and D at* 300 K

	NiF_2		CoF_2	
	A	*B*	*C*	*D*
Crystal volume (mm^3)	0.12×10^{-3}	2.0×10^{-3}	2.4×10^{-3}	1.5×10^{-3}
Scan speed (° min^{-1})	0.13–4.12	0.50–4.12	0.24–4.12	0.24–4.12
Scan width (°)	0.73–1.58	1.64–2.00	1.29–1.64	1.54–1.89
Detector aperture (mm)	(0.32–0.73) × 4.0	(1.91–2.96) × 4.0	(1.41–2.45) × 4.0	(1.91–2.95) × 4.0
$[(\sin\theta/\lambda)]_{max}$ ($Å^{-1}$)	1.074	1.074	1.073	1.073
Total No. of reflections	2570	2566	2872	2887
No. of reflections, $I > 3\sigma$	1557	1780	1549	1321
No. of independent reflections	137	154	140	137
Radiation	Mo $K\alpha$		Mo $K\alpha$	
Monochromator	Graphite (002)		Graphite (002)	
Scan type	ω–2θ		ω–2θ	
Take-off angle (°)	6.1		6.1	
Crystal-to-detector distance (mm)	173		173	

tuations all data were re-scaled against the appropriate standards.

Periodic checks of the orientation of the single crystals under investigation were made during the course of each experiment: after every set of six measurements the direction of the scattering vector for the current reflection was compared with that derived from a *UB* matrix. A maximum difference of 10% was allowed before reorientation of the crystal was considered necessary. However, this limit was never exceeded in any of the present data collections.

Data analysis

Data analysis was performed independently on data sets *A*, *B*, *C* and *D*, with *SDP* programs (Frenz, 1983) using a MicroVAX II with a VMS operating system.

Lorentz and polarization corrections appropriate to the current geometry were made. An absorption correction based on ψ scans of a few independent reflections with $80 < \chi < 90°$ and of their accessible equivalents was applied to data sets *B*, *C* and *D*, as suggested by North, Phillips & Mathews (1968). Based on results of a considerable number of previous measurements (Costa & Almeida, 1987), the authors believe that this method may be more reliable than the analytical absorption correction particularly for the very small specimens used in X-ray diffraction. The main reason for this preference is the fact that the ψ-scan technique is directly based on transmission data for the crystal under investigation and does not depend on any approximate estimation of its shape and volume. Owing to the small dimensions and irregular polyhedral shape of the crystals, the error involved in such an estimation may outweigh the advantages of an analytical correction.

This type of correction could not be applied to data set *A* because the orientation of the crystal was such that no satisfactory reflections (those with χ as close to 90° as possible) could be found. Instead a pathlength-dependent analytical correction was used for this data set (Coppens, Leiserowitz & Rabinovitch, 1965). Relevant data concerning the absorption corrections applied are given in Table 2.

Table 2. *Absorption correction data*

	NiF_2		CoF_2	
	A	*B*	*C*	*D*
Maximum absorption correction	0.8930	0.9983	0.9974	0.9983
Minimum absorption correction	0.8291	0.9463	0.9572	0.9192
Agreement factors (F_{obs}) (%)	1.5	1.5	1.8	2.5

Equivalent reflections were subsequently averaged; those for which $I_{hkl} \leq 3\sigma_{hkl}$ (σ_{hkl} being the standard deviation of I_{hkl}) were considered 'unobserved'.

Full-matrix least-squares refinements based on $(F_{obs} - F_{calc})^2$ were performed on each data set. A non-Poisson contribution weighting scheme was used where the weight w of each reflection is $w = 1/(\sigma_F)^2$ with $\sigma_F = \sigma_F{}^2/2F$ and $\sigma_F{}^2 = [\sigma_I^2 + (pF^2)^2]^{1/2}$. A value of 0.04 for the (instrumental) instability factor p was used to downweight the intense reflections. Other weighting schemes were tested, yielding no significant differences in the final results.

In the course of the refinement procedure sets of structure factors were calculated (F_{calc}), assuming spherical distributions of the atomic electrons. Anomalous-dispersion corrections were applied using data listed in the *International Tables for X-ray Crystallography* (1974, Vol IV).

One positional and six anisotropic thermal parameters U_{ij} (as defined in Almeida *et al.*, 1989) together with a scale factor were subsequently refined using high-order data, *i.e.* reflections with $(\sin\theta)/\lambda \geq 0.6$ $Å^{-1}$ (Stevens & Coppens, 1975).

Taking the structure amplitudes of all independent reflections (F_{obs}) as observables and fixing all the above parameters at the refined values to calculate a set of F_{calc}, an extinction parameter, g, was independently refined, using the approximate equation: $|F_c| = |F_{obs}|(1 + gI_c)$ (Stout & Jensen, 1968).

Values of the ratio F_{obs}^{corr}/F_{obs} are shown in Table 3 for sets of reflection intensities from crystals *A*, *B*, *C* and *D* with $w(F_{obs} - F_{calc}) \geq 2$.

Extinction is more severe for crystal *B* (NiF_2) than for any of the others as can be seen either comparing corresponding values of F_{obs}^{corr}/F_{obs} for different crystals or from the refined values of g. In fact the (110)

Table 3. *Ratios of observed structure-factor amplitudes after (F_{obs}^{corr}) and before (F_{obs}), the extinction correction*

hkl	Crystal *A*	Crystal *B*	Crystal *C*	Crystal *D*
110	52.51/36.42	54.22/30.30	49.58/37.72	49.44/36.24
011	34.82/29.77	34.48/26.51	32.42/28.95	33.04/29.01
020	23.20/21.77	21.90/19.63	20.84/19.99	20.57/19.62
111	—	22.04/20.00	—	—
121	42.73/37.00	40.97/31.91	40.14/36.14	39.53/35.08
220	46.54/39.40	46.57/34.95	45.47/40.28	—
002	51.01/42.17	50.88/36.96	50.48/43.51	50.86/42.99
130	28.97/27.30	27.55/24.77	—	—
112	33.61/31.15	32.60/28.55	—	—
031	44.84/39.49	42.88/34.41	41.17/37.53	41.73/37.57
040	30.22/28.80	28.80/26.42	—	27.64/26.63
222	34.34/32.40	32.70/29.65	—	—
330	33.36/31.57	24.10/22.93	—	—
141	—	23.11/22.08	—	—
240	—	26.33/25.13	—	—
332	—	26.03/24.92	—	
033	—	—	—	

Table 4. *Results of least-squares refinements based on reflections with* $\sin\theta/\lambda \geq 0.6$ Å^{-1} *from crystals A, B, C and D, and a representative example of several types of refinement for crystal B*

(*a*) Least-squares refinements

	NiF_2		CoF_2	
	Data set *A*	Data set *B*	Data set *C*	Data set *D*
F				
x	0.3036 (12)	0.3037 (2)	0.3033 (1)	0.3034 (1)
U_{11}	0.01025 (16)	0.00983 (20)	0.01263 (20)	0.01245 (23)
U_{33}	0.00691 (24)	0.00767 (29)	0.00839 (29)	0.01039 (40)
U_{12}	−0.00921 (46)	−0.00928 (82)	−0.01054 (56)	−0.00957 (78)
Ni / Co				
U_{11}	0.00526 (2)	0.00532 (4)	0.00696 (3)	0.00826 (3)
U_{33}	0.00423 (4)	0.00549 (8)	0.00518 (2)	0.00635 (8)
U_{12}	−0.00020 (42)	−0.00106 (23)	−0.00075 (62)	−0.00127 (65)
No. of reflections				
$\sin\theta/\lambda \geq 0.6$ Å^{-1}	99	113	101	99
$\sin\theta/\lambda \geq 0.1$ Å^{-1}	137	154	140	137
R (%)	1.3	2.0	1.9	1.6
wR (%)	1.7	2.2	2.6	1.7
S	0.369 (1)	0.189 (2)	0.373 (4)	0.436 (2)
$g \times 10^5$	3.74 (7)	6.79 (9)	2.88 (6)	3.36 (6)

(*b*) Refinements for crystal *B*

Refinement based on	$I > 3\sigma^*$	$I > \sigma^*$	$I > \sigma^*$	$I > 3\sigma$
	F	F	F^2	F
Atom	F	F	F	F
x	0.30373 (24)	0.30361 (22)	0.30357 (22)	0.30373 (24)
U_{11}	0.00983 (20)	0.00992 (18)	0.00998 (19)	0.00983 (20)
U_{33}	0.00767 (29)	0.00767 (26)	0.00766 (26)	0.00767 (29)
U_{12}	−0.00928 (82)	−0.00915 (71)	−0.00907 (71)	−0.00928 (82)
Atom	Ni	Ni	Ni	Ni
U_{11}	0.00532 (4)	0.00529 (4)	0.00528 (4)	0.00532 (4)
U_{33}	0.00549 (8)	0.00545 (7)	0.00542 (7)	0.00549 (8)
U_{12}	−0.00106 (23)	0.00086 (19)	0.00081 (19)	−0.00106 (23)
No. of reflections				
$\sin\theta/\lambda \geq 0.6$ Å^{-1}	113	138	138	113
$\sin\theta/\lambda \geq 0.1$ Å^{-1}	153	178	178	154
R (%)	1.5	1.7		2.0
wR (%)	2.5	2.4		2.2
S	0.189 (2)	0.189 (2)	0.190 (2)	0.189 (2)
$g \times 10^5$	8.04 (10)	7.87 (13)	7.83 (13)	6.79 (9)

*(110) reflection rejected.

reflection is exceptionally extinguished in this crystal ($F_{obs}^{corr}/F_{obs} = 0.56$); this ratio varies between 0.73 and 0.88 for five other reflections, being higher than 0.88 for the remaining so-called 'extinguished reflections' shown in Table 3. Furthermore, comparing the results for crystals *A* and *B*, the averaged ratio of the corresponding F_{obs}^{corr} is 1.030 with an e.s.d. of 0.027. If reflection (110) is excluded from the refinement no significant variation is found in the *R* factors [the atomic parameters do not change since they are refined from data with $(\sin\theta)/\lambda \geq 0.6$ Å^{-1})]; however, the extinction parameter, *g*, increases about 20% and the averaged ratio of the F_{obs}^{corr} for crystals *A* and *B* becomes 1.002 with a smaller e.s.d. (less than 2% for the high intensities). Therefore, in the final refinement of the extinction parameter and in the subsequent calculation of Fourier maps for crystal *B* this reflection was rejected.

Extinction appears to be adequately corrected for in crystals *C* and *D* (CoF_2), the average ratio of the corresponding F_{obs}^{corr} being 0.998, with an e.s.d. not higher than 1%.

Similar refinements to those described above have been carried out based on reflections with $I_{hkl} \geq \sigma_{hkl}$

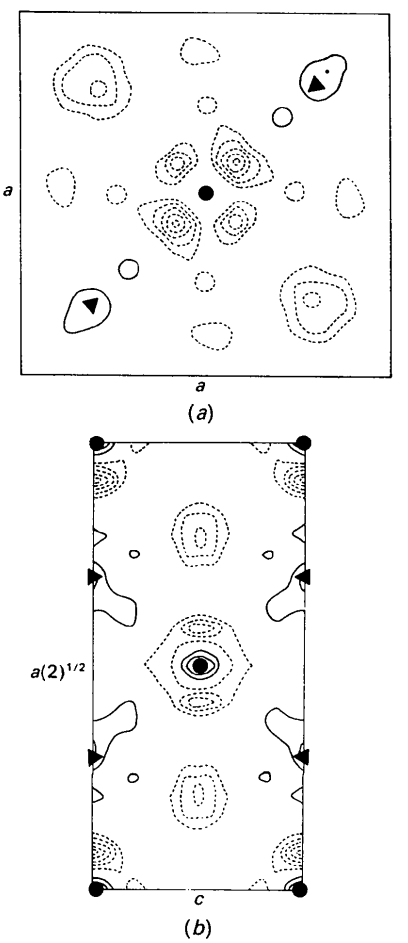

Fig. 2. Difference Fourier maps for crystal *A* (NiF_2); contour intervals at 0.2 e Å^{-3}. Solid and dashed lines represent positive and negative contours, respectively. Standard deviation of constant regions: 0.16 e Å^{-3}. (*a*) [001] section; (*b*) [110] section. ● = Ni atoms, ▲ = F atoms.

in order to test the influence of weak reflections. Refinements on F^2 have also been attempted. In all types of refinement the results for all crystals agree well within the errors.

All refinements were carried out until a shift/e.s.d. ratio smaller than 0.001 was achieved for all the parameters refined.

A summary of the data referring to refinements with $I_{hkl} \geq 3\sigma_{hkl}$ for all the crystals is given in Table 4(*a*). Table 4(*b*) is a representative example of several other types of refinement for crystal *B*.

Difference density maps

The results of Fourier inversion of each data set, $(F_{obs} - F_{calc})$, can be visualized in terms of the difference density maps for convenient sections of the unit cell as shown in Figs. 2 and 3 for NiF_2, and in Figs. 4 and 5 for CoF_2. Fig. 6 is a representative example of the corresponding error maps; the standard deviation for constant regions is typically of the order of 0.16 e $Å^{-3}$.

(*a*) NiF_2

Difference maps for both crystals show a few similarities which are likely to represent real effects in the charge density distribution: a negative density of about 1 e $Å^{-3}$ is always observed around the metal atom as can be seen both on section [001] and [110]. This indicates a deficiency of electrons in the vicinity of the Ni atom. The missing electrons are partly transferred to the F atom as evidenced by one positive contour along the directions joining metal and ligand atoms, the estimated value of the charge transferred being about 0.2 e $Å^{-3}$.

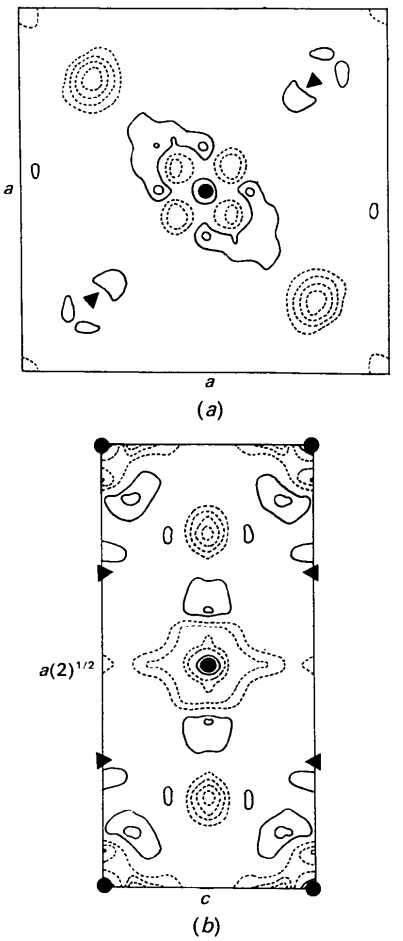

Fig. 3. Difference Fourier maps for crystal *B* (NiF_2); contour intervals at 0.2 e $Å^{-3}$. Solid and dashed lines represent positive and negative contours, respectively. Standard deviation of constant regions: 0.17 e $Å^{-3}$. (*a*) [001] section; (*b*) [110] section. ● = Ni atoms, ▲ = F atoms.

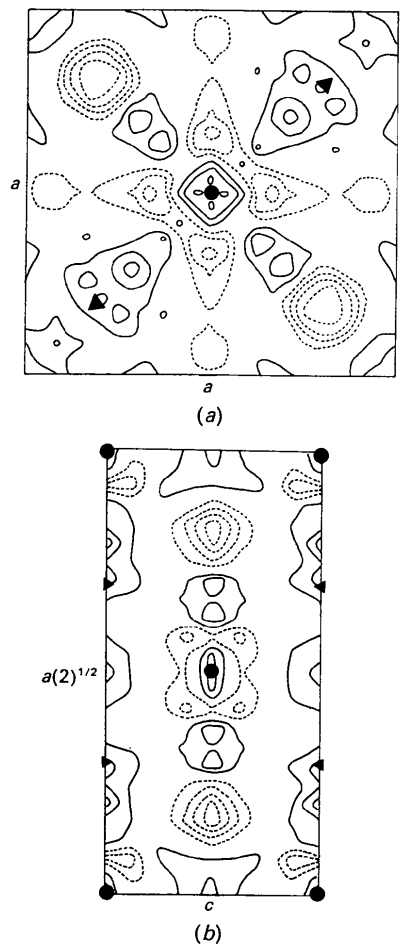

Fig. 4. Difference Fourier maps for crystal *C* (CoF_2); contour intervals at 0.2 e $Å^{-3}$. Solid and dashed lines represent positive and negative contours, respectively. Standard deviation of constant regions: 0.19 e $Å^{-3}$. (*a*) [001] section; (*b*) [110] section. ● = Co atoms, ▲ = F atoms.

(*b*) CoF_2

A deficiency of about 0.8 e $Å^{-3}$ near the Co atom can also be observed on both crystals. Some of these electrons appear to be preferentially distributed along [001] directions, between two nearest metal atoms, which are second-nearest neighbours in the structure. This effect, which can be observed on the section [110], has also been detected in VF_2 and FeF_2 (Costa & Almeida, 1987; Almeida *et al.*, 1989).

Charge density analysis in terms of 3*d* atomic orbitals

The results described in the previous section were interpreted in terms of fractional occupation of 3*d* orbitals, assuming that the significant contour levels observed in the difference density maps represent the eventual asphericity of the 3*d* charge density distribution caused by a crystal field with tetragonal symmetry. Although this is not strictly true – the actual symmetry of the crystal field is orthorhombic as can be seen from the geometry of the environment of each transition metal in Fig. 1 – the approximation is valid, since the distortion is small. This can be confirmed by the values of the F—*M*—F (*M* = Ni, Co) angle which differs from 90°: 79.9° for NiF_2 and 78.6° for CoF_2.

The assumption of tetragonal symmetry implies that d_{xz} and d_{yz} orbitals are symmetry equivalent. Therefore, only the fractional occupations of d_{z^2}, $d_{x^2-y^2}$ and d_{xy} orbitals, α_1, α_2 and α_3, respectively, were refined independently; the equal population of the remaining *d* orbitals was taken as $\alpha_4 = \alpha_5 = [1-(\alpha_1+\alpha_2+\alpha_3)]/2$.

The comparison of the observed 3*d* charge density with that deduced from 3*d* atomic orbitals was made in terms of structure-factor amplitudes – the directly observed quantities – as explained in detail elsewhere (Costa & Almeida, 1987; Almeida *et al.*, 1989).

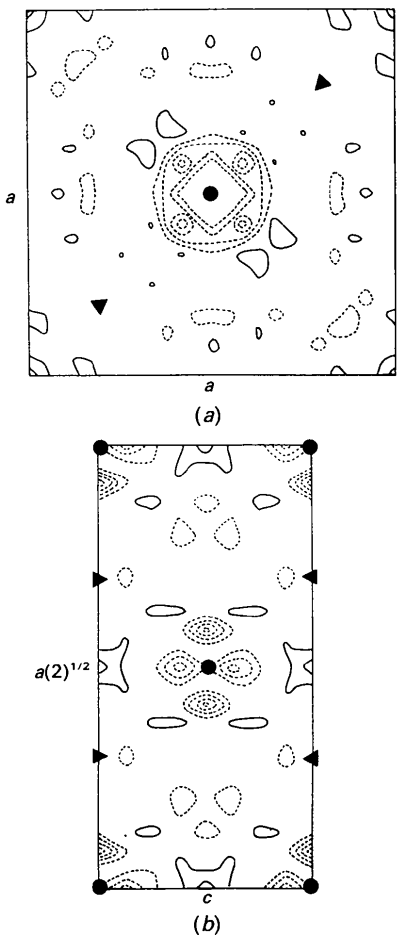

Fig. 5. Difference Fourier maps for crystal *D* (CoF_2); contour intervals at 0.2 e $Å^{-3}$. Solid and dashed lines represent positive and negative contours, respectively. Standard deviation of constant regions: 0.14 e $Å^{-3}$. (*a*) [001] section; (*b*) [110] section. ● = Co atoms, ▲ = F atoms.

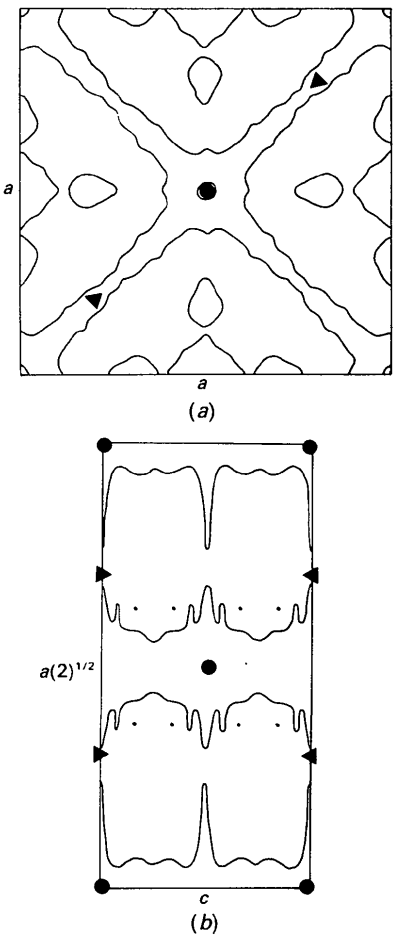

Fig. 6. Fourier maps representing the distribution of errors in difference density for crystal *A* (NiF_2); contours at 0.2 e $Å^{-3}$. (*a*) [001] section; (*b*) [110] section. ● = Ni atoms, ▲ = F atoms.

The results of a least-squares analysis are given in Table 5 (for definitions of goodness-of-fit parameters χ_s^2 and χ_a^2 see Almeida *et al.*, 1989).

The agreement factors for any two crystals of the same material are satisfactory.

Although the asphericity of 3*d* electrons both in CoF_2 and NiF_2 is hardly significant, as confirmed by the χ^2 values obtained, the overall results indicate a very slight deficiency of electrons in d_{z^2} orbitals of NiF_2 and in d_{xy} orbitals of CoF_2.

The aim of a refinement of 3*d*-orbital polulations is to provide a direct and easily visualized picture of any asphericity in the distribution of 3*d* electrons, evidenced by preferencial occupancy of orbitals directed towards F atoms.

Multipole refinement

Using the least-squares program *MOLLY* (Hansen & Coppens, 1978) the observed structure-factor amplitudes for specimens *A*, *B*, *C* and *D* were compared with those derived from a superposition of atomic densities expanded in series of real spherical harmonics (Almeida *et al.*, 1989). Radial form factors tabulated by Clementi & Roetti (1974) were used in the calculation of model structure factors.

Positional, thermal and extinction parameters [Becker & Coppens (1975) model, with Lorentzian distribution of domains and an averaged pathlength included] were refined simultaneously with a scale factor and multipole population parameters. For the transition metal, Ni or Co, all multipole populations up to $l = 4$, compatible with the local symmetry, were refined. The electron density at any point in the unit cell was taken as a sum of a spherical contribution of the core and the valence electrons [*i.e.* argon core, $4s^2$ for Ni and Co and $1s^2$ for F] and the total contribution (both spherical and aspherical) of the remaining electrons (Almeida *et al.*, 1989). Therefore the term of the expansion containing P_{00} refers to the sperical contribution of the (3*d*) electrons of the metal atom and the (2*s*2*p*) electrons of the F atom. Only P_{00} was refined for the ligand atom, since one expects the small asphericity observed in the charge distributions of NiF_2 and CoF_2 to be mainly as a result of the 3*d* electrons of the metal atom. This appears to be a justifiable assumption for ions like F^- with closed-shell configurations; moreover, it contributes to keeping the number of refined parameters as low as possible, thus avoiding undesirable correlations. In the present analysis the following correlations were found to exceed 70%: between U_{12} and P_{22} for the metal ion (crystals *A*, *C* and *D*); between P_{40} and P_{42} for Co (crystals *C* and *D*); and between scale and extinction parameters for crystal *B*.

Table 5. *Fractional occupancies of* 3*d orbitals obtained from least-squares refinement and multipole refinement*

(*a*) Least-squares refinement

		α_1	α_2	α_3	$\alpha_4 = \alpha_5$	χ_s^2	χ_a^2
NiF_2	*A*	0.15 (2)	0.22 (2)	0.17 (2)	0.23 (3)	2.4	3.2
	B	0.16 (3)	0.26 (3)	0.23 (3)	0.18 (5)	7.1	6.2
CoF_2	*C*	0.22 (2)	0.16 (3)	0.16 (3)	0.23 (5)	2.3	2.3
	D	0.18 (3)	0.22 (3)	0.15 (3)	0.23 (5)	3.6	3.7

(*b*) Multipole refinement

		α_1	α_2	α_3	α_4	α_5
NiF_2	*A*	0.11 (2)	0.24 (2)	0.11 (2)	0.21 (2)	0.29 (2)
	B	0.09 (3)	0.22 (3)	0.13 (3)	0.25 (3)	0.24 (3)
CoF_2	*C*	0.19 (6)	0.09 (7)	0.21 (7)	0.21 (7)	0.27 (7)
	D	0.13 (6)	0.20 (7)	0.24 (7)	0.17 (7)	0.22 (7)

Table 6. *Results of multipole refinements for* NiF_2 *and* CoF_2

The coefficients P_{ij} refer to the contribution of the (3*d*) electrons for Ni and Co and to the (2*s*2*p*) electrons for F, as mentioned in the text.

(*a*) NiF_2

	Crystal *A*		Crystal *B*	
	Ni	F	Ni	F
x	—	0.30369 (7)	—	0.30356 (12)
U_{11}	0.00556 (4)	0.01023 (11)	0.00529 (8)	0.01023 (16)
U_{33}	0.00418 (6)	0.00719 (15)	0.00556 (13)	0.00778 (20)
U_{12}	−0.00140 (60)	−0.00870 (26)	−0.00066 (56)	−0.00843 (44)
P_{00}	0.970 (6)	1.780 (6)	0.942 (12)	1.808 (12)
P_{20}	0.005 (9)		−0.005 (9)	
P_{22}	−0.018 (6)		0.010 (8)	
P_{40}	−0.063 (5)		−0.066 (6)	
P_{42}	−0.020 (4)		−0.005 (6)	
P_{44}	0.0041 (5)		0.028 (6)	
R (%)	1.7		1.1	
wR (%)	2.3		1.4	
S	2.806 (5)		5.460 (19)	
Mosaic spread	14.31′		20.25′	
Domain radius (nm)	289		204	

(*b*) CoF_2

	Crystal *C*		Crystal *D*	
	Co	F	Co	F
x	—	0.30346 (19)	—	0.30341 (17)
U_{11}	0.00739 (11)	0.01320 (28)	0.00827 (11)	0.01298 (20)
U_{33}	0.00602 (16)	0.00879 (39)	0.00591 (16)	0.01021 (32)
U_{12}	−0.00308 (237)	−0.01024 (85)	−0.00008 (222)	−0.01024 (74)
P_{00}	0.803 (12)	1.821 (12)	0.842 (8)	1.782 (8)
P_{20}	0.028 (28)		−0.030 (28)	
P_{22}	−0.011 (18)		−0.002 (16)	
P_{40}	−0.044 (19)		−0.019 (20)	
P_{42}	−0.018 (16)		−0.019 (16)	
P_{44}	−0.039 (21)		−0.013 (19)	
R (%)	1.4		1.34	
wR (%)	1.6		1.43	
S	2.811		2.334 (12)	
Mosaic spread	0.88′		0.78′	
Domain radius (nm)	77		88	

The results of the multipole refinements carried out on each data set are shown in Table 6(*a*) for NiF_2 and in Table 6(*b*) for CoF_2. Positional and thermal parameters are to be compared with those given in Table 4(*a*): corresponding values agree within one (or a few) standard deviations. Moreover, results for different crystals of the same compound agree within less than three standard deviations.

Aspherical multipole populations for similar crystals agree within less than two standard deviations. It can be noticed that only P_{40} and P_{44} for NiF_2 are significantly different from zero in both data sets.

Concluding remarks

The results of multipole analysis can also be interpreted in terms of 3*d*-orbital occupancies α_i ($i = 1, 5$) using generalized relations derived by Holladay, Leung & Coppens (1983), as described elsewhere (Almeida *et al.*, 1989). For the present case these are given in Table 5(*b*).

Comparison of corresponding values of α_i's derived from the different models considered, namely 3*d* atomic orbitals and multipole functions, is not strictly valid, because the models are not based on the same assumptions. In fact, the condition of tetragonal symmetry – which is in itself an approximation to the true orthorhombic symmetry – is not imposed on the multipole refinement; moreover, this type of analysis allows for charge transfer between the metal and ligand ions which is in no way taken into account by the model based on atomic orbitals.

Such arguments may lead to the conclusion that the α_i values derived from a multipole analysis are more liable to reproduce the real situation for the charge density in the structures investigated. It should also be noted that whereas the α_i's in Table 5(*a*) were refined from sets of data (F^{3d}_{obs}) which were determined by the results of a previous spherical refinement (positional and thermal parameters, scale and extinction factors), the corresponding α_i's in Table 5(*b*) are refined together with all parameters, the results showing no significant correlations.

Taking into account the multiplicities of the metal and ligand ions in the rutile structure, 0.125 and 0.25, respectively, and the number of electrons outside closed shells, the expected values for P_{00} in the absence of charge transfer would be:

(i) Ni ($3d^8$) $P_{00} = 8 \times 0.125 = 1.00$
(ii) Co ($3d^7$) $P_{00} = 7 \times 0.125 = 0.875$
(iii) F ($2s^2 + 2p^5$) $P_{00} = 7 \times 0.250 = 1.75$

In the case of CoF_2 there is a slight charge transfer from the metal to the ligand as evidenced by the values of P_{00} shown in Table 6, for both crystals, in comparison to those expected. The same conclusion applies to the case of NiF_2: a decrease of P_{00} from the above values for the metal ion is balanced by an increase in P_{00} for the ligand, preserving the unit-cell neutrality.

The analysis of asphericities in the charge density is not very conclusive since, as could be seen both in the Fourier maps and in the course of the refinement of the α_i parameters, these are hardly significant. However, giving slightly more credit to the results of Table 5(*b*) (as explained above) without neglecting the information contained in Table 5(*a*), one may conclude that there is some depletion of d_{z^2} and d_{xy} orbitals in NiF_2. The same overall effect is not obvious in CoF_2 from a combined analysis of Tables 5(*a*) and 5(*b*).

Table 7. *Metal–ligand distances in rutile structures*

$d_1 = |\mathbf{r}_{x,x,0} - \mathbf{r}_{000}|$; $d_2 = |\mathbf{r}_{(1/2)+x,(1/2)-x,(1/2)} - \mathbf{r}_{000}|$.

	VF_2	MnF_2	FeF_2	CoF_2	NiF_2
d_1 (Å)	2.075 (6)	2.114 (4)	2.003 (1)	2.014 (1)	1.997 (1)
d_2 (Å)	2.091 (5)	2.122 (2)	2.117 (1)	2.058 (1)	2.011 (1)
d_{FF} (Å)	2.626 (18)	2.639 (3)	2.621 (3)	2.612 (3)	2.582 (6)

A few final conclusions can be drawn from an overall analysis of the deviations from a free-ion configuration, along the MF_2 series of rutiles (M = V, Mn, Fe, Co, Ni).

Covalency effects are more significant towards the end of the series for those rutile structures with 3*d*-electron configurations deviating more markedly from the half-closed shell configuration of Mn, namely for CoF_2 and NiF_2. Such effects are hardly noticeable in FeF_2 and in MnF_2 as confirmed by neutron diffraction data obtained for this compound (Andrade, 1986).

Moreover, covalency in the series investigated also appears to be related to the average metal–ligand distance, shown in Table 7, being more significant in the structures in which such a distance is smaller.

Common asphericity effects could be found along the series, namely the depletion of d_{z^2} orbital population, which is most striking in the case of VF_2 and MnF_2. It should be noted that these two structures have comparatively high unit-cell volumes. One may thus infer that 3*d* electrons tend to 'avoid' metal–ligand bonding directions in those structures where the degree of packing allows them to redistribute either along or in between other bonding directions.

We are indebted to the Cultural Service of the German Federal Republic Embassy, the Deutscher Akademischer Austauschdienst (DAAD) and the German Agency for Technical Cooperation (GTZ) for the offer of a CAD-4 automatic diffractometer which enabled the experimental work to be carried out.

References

ALMEIDA, M. J. M., COSTA, M. M. R. & PAIXÃO, J. A. (1989). *Acta Cryst.* B**45**, 549–555.
ANDRADE, L. C. R. (1986). PhD dissertation, Univ. of Coimbra, Portugal.
BECKER, P. J. & COPPENS, P. (1975). *Acta Cryst.* A**31**, 417–425.
CLEMENTI, E. & ROETTI, C. (1974). *At. Data Nucl. Data Tables*, **14**(3), 4.
COPPENS, P., LEISEROWITZ, L. & RABINOVITCH, D. (1965). *Acta Cryst.* **18**, 1035–1038.
COSTA, M. M. R. & ALMEIDA, M. J. M. (1987). *Acta Cryst.* B**43**, 346–352.
FRENZ, B. A. (1983). *Enraf–Nonius Structure Determination Package*; *SDP Users Guide*. Version of 6 January 1983. Enraf–Nonius, Delft, The Netherlands.
HAENDLER, H. M., PATTERSON, W. L. & BERNARD, W. J. (1952). *J. Am. Chem. Soc.* **74**, 3167–3168.

HANSEN, N. K. & COPPENS, P. (1978). *Acta Cryst.* A**34**, 909–921.
HOLLADAY, A., LEUNG, P. & COPPENS, P. (1983). *Acta Cryst.* A**39**, 377–387.
NORTH, A. C. T., PHILLIPS, D. C. & MATHEWS, F. S. (1968). *Acta Cryst.* A**24**, 351–359.
STEVENS, E. D. & COPPENS, P. (1975). *Acta Cryst.* A**31**, 612–619.
STOUT, G. H. & JENSEN, L. H. (1968). *X-ray Structure Determination*, pp. 410–412. London: Macmillan.
STOUT, J. W. & REED, S. A. (1954). *J. Am. Chem. Soc.* **76**, 5279–5281.

Acta Cryst. (1993). B**49**, 599–604

Defect Structure and Diffuse Scattering of Zirconia Single Crystals Doped with 7 mol% CaO

BY TH. PROFFEN, R. B. NEDER AND F. FREY

Institut für Kristallographie und Mineralogie, Theresienstrasse 41, 8000 *München* 2, *Germany*

AND W. ASSMUS

Physikalisches Institut der Universität Frankfurt, Germany

(*Received* 21 *September* 1992; *accepted* 4 *January* 1993)

Abstract

The defect structure of 7 mol% calcium-stabilized zirconia (CSZ) is described in terms of a correlated distribution of microdomains within the cubic matrix of CSZ. It is shown that the defect structure is very similar to that of 15 mol% CSZ. The defect structure consists of two types of defects: microdomains based on a single oxygen vacancy with relaxed neighbouring ions and microdomains based on a pair of oxygen vacancies separated by $a3^{1/2}/2$ along $\langle 111 \rangle$. Calculations show that a tetragonal distortion cannot explain the observed diffuse scattering. Several arguments suggest that the defect structure is not that of the Φ_1 phase: first, the similarity of diffuse scattering of yttrium-stabilized zirconia, for which no Φ_1 phase exists; second, the diffuse scattering of CSZ is almost identical from 4 mol% CSZ up to 20 mol% CSZ; third, the diffuse scattering is temperature dependent; and fourth, a direct comparison of single-crystal intensities of the Φ_1 phase with the intensity of diffuse scattering.

Introduction

Pure cubic zirconia is thermodynamically stable only at temperatures above 2643 K. Below this temperature a tetragonal phase is stable down to 1200–1300 K. At room temperature a monoclinic phase is the stable polymorph. An average fluorite structure of zirconia can, however, be stabilized at room temperature by doping with oxides of various di- and trivalent metals such as Ca, Mg, Y and Yb. This cubic phase is stable over a range of compositions. The exact mechanism of the stabilization and the solution of the structure of the solid has been the scope of several investigations (Neder, Frey & Schulz, 1990*b*, and references therein). Neder *et al.* (1990*b*) showed that the disordered diffuse scattering of cubic zirconia stabilized by 15 mol% CaO (CSZ15) can be analyzed by the correlated distribution of microdomains* within a matrix of cubic zirconia.

There is, however, still a controversial debate concerning whether the diffuse scattering of calcium-stabilized zirconia (CSZ) may be analyzed equally well by microdomains within the Φ_1 structure (Rossell, Sellar & Wilson 1991; Rossell, 1992) or by locally ordered arrangements with tetragonal symmetry (Martin, Boysen & Frey, 1993; Andersen, Clausen, Hackett, Hayes, Hutchings, Macdonald & Osborn, 1986; Osborn, Andersen, Clausen, Hackett, Hayes, Hutchings & Macdonald, 1986). The relevant results obviously depend sensitively on the type of sample, *i.e.* single crystal or powder.

To clarify these points further, and to see how the defect structure changes with composition we have investigated the diffuse scattering of single crystals with 7 mol% CaO (CSZ7). The results should give an important insight into the stabilizing mechanism. Proffen, Neder, Frey, Keen & Zeyen (1993) deal with the temperature dependence of diffuse scattering in CSZ with different amounts of CaO.

* The terms 'domain' or 'microdomain' are used in this paper, because it is the usual terminology in this context. We are well aware that this terminology does not match the strict crystallographic definition of a domain.